

Detecting Galaxy-Filament Alignments in the Sloan Digital Sky Survey III

Yen-Chi Chen,¹* Shirley Ho,^{2,3,4} Jonathan Blazek^{5,6}, Siyu He,^{2,3,4} Rachel Mandelbaum,^{3,4} Peter Melchior,⁷ Sukhdeep Singh^{8,2,3,4}

¹Department of Statistics, University of Washington, Seattle, WA 98195, USA

²Lawrence Berkeley National Lab, Berkeley, CA 94720, USA

³Department of Physics, Carnegie Mellon University, Pittsburgh, PA 15213, USA

⁴McWilliams Center for Cosmology, Carnegie Mellon University, Pittsburgh, PA 15213, USA

⁵Institute of Physics, Laboratory of Astrophysics, École Polytechnique Fédérale de Lausanne (EPFL), 1290 Versoix, Switzerland

⁶Center for Cosmology and AstroParticle Physics, Department of Physics, Ohio State University, Columbus, OH 43210, USA

⁷Department of Astrophysical Sciences, Princeton University, Princeton, NJ, 08544, USA

⁸Berkeley Center for Cosmological Physics and Department of Physics, University of California, Berkeley, CA 94720

22 February 2019

ABSTRACT

Previous studies have shown the filamentary structures in the cosmic web influence the alignments of nearby galaxies. We study this effect in the LOWZ sample of the Sloan Digital Sky Survey using the “Cosmic Web Reconstruction” filament catalogue. We find that LOWZ galaxies exhibit a small but statistically significant alignment in the direction parallel to the orientation of nearby filaments. This effect is detectable even in the absence of nearby galaxy clusters, which suggests it is an effect from the matter distribution in the filament. A nonparametric regression model suggests that the alignment effect with filaments extends over separations of 30 – 40 Mpc. We find that galaxies that are bright and early-forming align more strongly with the directions of nearby filaments than those that are faint and late-forming; however, trends with stellar mass are less statistically significant, within the narrow range of stellar mass of this sample.

Key words: (cosmology:) large-scale structure of Universe

1 INTRODUCTION

Cosmological simulations of large-scale structure reveal a consistent picture for the alignments of dark matter halo shapes and spins with filaments (for a review of galaxy and halo alignments, see Joachimi et al. 2015). The fact that filaments are associated with the large-scale tidal field (Hahn et al. 2007a,b; Sousbie et al. 2008; Forero-Romero et al. 2009; Aragón-Calvo et al. 2010; Cautun et al. 2013), which directly sources the dark matter halo spins through tidal torquing and imprints coherent patterns in their shapes, makes this connection quite natural and unsurprising. For details of how dark matter halo spins and shapes align with filamentary structures, and the dependence on other properties such as halo mass, see for example Altay et al. (2006); Aragón-Calvo et al. (2007); Hahn et al. (2007c); Zhang et al. (2009); Libeskind et al. (2013); Aragon-Calvo & Yang (2014); Ganeshiah Veena et al. (2018).

However, the expectations for galaxy (not halo) shape

and spin alignments are less obvious, and the observational results are somewhat in conflict with each other. For example, Tempel & Libeskind (2013) and Zhang et al. (2015) reported contradictory results for the alignments of spiral galaxy spins with filaments. The differing results may arise due to differences in sample selection, spin measurement, or mass ranges.

In this work, rather than investigate galaxy *spin* alignments with filaments, we focus on galaxy *shape* alignments with filaments. The primary motivation behind considering shape alignments is that coherent galaxy shape alignments with the cosmic web are a contaminant to weak gravitational lensing measurements (for recent reviews, see Kilbinger 2015; Mandelbaum 2017) that serve as one of the most promising probes of dark energy. Weak gravitational lensing involves statistical measurements of low-level coherent galaxy shape distortions induced by the gravitational potential of large-scale structure, and hence “intrinsic alignments” (coherent alignments due to large-scale tidal fields) must be modeled and removed. There are several approaches to modeling these alignments: to date, most cosmological

* E-mail: yenchic@uw.edu

weak lensing analyses (e.g., [DES Collaboration et al. 2017](#); [Hildebrandt et al. 2017](#)) have used numerical models for intrinsic alignments that should be valid only to mildly nonlinear scales. More sophisticated analytic modeling schemes have been developed, some with additional nonlinear terms (e.g., [Blazek et al. 2017](#)), which can include the impact of spin alignments, and others based on the inclusion of a halo model for the effects that arise inside of dark matter halos ([Schneider & Bridle 2010](#)). It is important to understand whether galaxy shapes are aligned with filaments in a way that requires inclusion of additional terms in these models in order to properly remove intrinsic alignments contamination from future weak lensing measurements.

In this paper, we study the effect from filaments on galaxy shape alignments using the LOWZ sample in the Sloan Digital Sky Survey (SDSS). We acquire filaments from the cosmic web reconstruction catalogue ([Chen et al. 2016](#)) and use a catalogue of galaxy shapes measured using the re-Gaussianization method ([Hirata & Seljak 2003](#)). Our results can be compared with a similar analysis using the same filament-finding method in cosmological hydrodynamic simulations ([Chen et al. 2015c](#)). In addition to following previous works in quantifying how galaxy-filament alignments scale with galaxy properties, we also attempt to separate out the impact of filaments on galaxy alignments from the impact of clusters on galaxy alignments.

The outline of the paper is as follows. After describing the data used for this work in [Section 2](#), we show the impact of filaments on galaxy-cluster alignments in [Section 3.1](#). In [Section 3.2](#), we measure galaxy-filament alignments after accounting for the alignment of galaxies towards clusters. We study how galaxy-filament alignments scale with separation as well as the impact of different galaxy properties. Finally, we conclude in [Section 4](#).

Throughout the paper, we assume a WMAP7 Λ CDM cosmology with $H_0 = 70$ km/s/Mpc, $\Omega_m = 0.274$, and $\Omega_\Lambda = 0.726$ ([Komatsu et al. 2011](#)) and use angular diameter distances for calculation of physical distances.

2 DATA

2.1 The Sloan Digital Sky Survey

The SDSS ([York et al. 2000](#)) imaged roughly π steradians of the sky, with the imaging carried out by drift-scanning the sky in photometric conditions ([Hogg et al. 2001](#); [Ivezić et al. 2004](#)), in five bands (*ugriz*) ([Fukugita et al. 1996](#); [Smith et al. 2002](#)) using a specially-designed wide-field camera ([Gunn et al. 1998](#)) on the SDSS Telescope ([Gunn et al. 2006](#)). These imaging data were used to create the catalogues of galaxy shapes that we use in this paper. The SDSS-I/II imaging surveys were completed with a seventh data release ([Abazajian et al. 2009](#)), though this work will rely as well on an improved data reduction pipeline that was part of the eighth data release, from SDSS-III ([Aihara et al. 2011](#)); and an improved photometric calibration (‘ubercalibration’, [Padmanabhan et al. 2008](#)).

2.2 Baryon Oscillation Spectroscopic Survey (BOSS)

Based on the photometric catalog from SDSS, galaxies are selected for spectroscopic observation ([Dawson et al. 2013](#)), and the BOSS spectroscopic survey was performed ([Ahn et al. 2012](#)) using the BOSS spectrographs ([Smee et al. 2013](#)). Targets are assigned to tiles of diameter 3° using an adaptive tiling algorithm ([Blanton et al. 2003](#)), and the data were processed by an automated spectral classification, redshift determination, and parameter measurement pipeline ([Bolton et al. 2012](#)).

We use SDSS-III BOSS data release 12 (DR12; [Alam et al. 2015](#)) LOWZ galaxies. This sample consists of 361,762 galaxies over an area of 8377 deg² ([Reid et al. 2016](#)). We use these galaxies to construct an overdensity map from which we construct the filament map.

To get the shapes of BOSS galaxies, we use the same shape catalog as was used in [Singh et al. \(2015\)](#). The galaxy shapes were measured by [Reyes et al. \(2012\)](#) using the re-Gaussianization method ([Hirata & Seljak 2003](#)) of correcting for the effects of the point-spread function (PSF) on the observed galaxy shapes. We refer the reader to [Singh et al. \(2015\)](#) and [Reyes et al. \(2012\)](#) for further details of the shape measurements.

We also use galaxy clusters from the redMaPPer catalogue version 10 ([Roza & Rykoff 2014](#); [Rykoff et al. 2014](#); [Roza et al. 2015](#)) to test the effects of clusters on the galaxy alignments. In addition we also use publicly-available estimates¹ of galaxy stellar mass and age based on the Flexible Stellar Population Synthesis code of [Conroy et al. \(2009\)](#), in order to test the impact of these properties on galaxy alignments.

2.3 Filament Catalogue

We obtain filaments from the *Cosmic Web Reconstruction*² catalogue ([Chen et al. 2016](#)), a publicly-available filament catalogue consisting of filaments in SDSS from redshift $z = 0.05$ to $z = 0.70$. Note that in this paper, we only use the LOWZ sample, so we restrict ourselves to $0.20 < z < 0.43$.

The catalogue is constructed by first slicing the spectroscopic galaxy sample from redshift $z = 0.05$ to $z = 0.70$ into 130 thin slices along line of sight with width $\Delta z = 0.005$ and then projecting galaxies within each slice onto two dimensional plane of RA, DEC (denoted as x in following discussion). The galaxies in the same slice are then smoothed into a two dimensional probability density field, $p(x)$ using a Gaussian kernel $K(x)$

$$p(x) = \frac{1}{nh^2} \sum_{\ell=1}^n K\left(\frac{x - x^\ell}{h}\right) \quad (1)$$

with the smoothing bandwidth $h > 0$ chosen by the reference rule described in [Chen et al. \(2015b\)](#). In the LOWZ sample, h ranges from 20 – 40 Mpc. Finally, we detect the filaments as the ridges of the density field ([Chen et al. 2015a](#)) using the subspace constrained mean shift algorithm ([Ozertem & Erdogmus 2011](#)).

¹ http://www.sdss.org/dr12/spectro/galaxy_granada/

² <https://sites.google.com/site/yenchicr/>

Note that the density field $p(x)$ is constructed assuming a flat space geometry (i.e., we do not take into account the fact that the RA-DEC coordinate is curved) so there will be some systematics caused by ignoring this geometry. However, such systematics are very tiny because our smoothing scale is about 1–2 degrees. For a Gaussian kernel, contribution from 3σ away has a value less than $1/8000$ so they are negligible in the analysis. This suggests that the systematics from geometry is at the scale of comparing a short arc of 3–6 degrees to a straight line connect the two ends of the arc. This difference is $|\sin(\frac{6^\circ}{2}) - \frac{6^\circ}{2}| \approx (\frac{\pi}{60})^3 \approx 10^{-3} = 0.1\%$. So the systematics from ignoring the geometry will not impact much on the density field $p(x)$.

The ridges are identified using the hessian of the density field (tidal tensor), $H_{ij}(x) = \frac{\partial^2}{\partial x_i \partial x_j} p(x)$ with $v_1(x), v_2(x)$ as its eigenvectors corresponding to the eigenvalues $\lambda_1(x) \geq \lambda_2(x)$. The ridges are defined as

$$R = \left\{ x : v_2(x)^T \nabla p(x) = 0, \lambda_2 < 0 \right\}, \quad (2)$$

where $\nabla p(x)$ is the gradient of the density field. R is the collection of points where the gradient projected onto the subspace spanned by the second eigenvector $v_2(x)$ is zero and the second eigenvalue is negative. This implies that every point on R is a local maximum in the subspace spanned by $v_2(x)$, so R can be viewed as a curve consisting of many local maxima in some subspaces, which is the feature of a ridgeline.

Note that ridges (hereafter filaments) are 1-dimensional objects (curves), so we can easily define the orientation of every point on a filament. In reality, a filament is represented by a collection of points and every point contains a vector η_{filament} indicating the orientation of the filament passing through the point. Points on filaments are created from applying the ridge finding algorithm (the subspace constrained mean shift algorithm) to a uniform 2D grid. Roughly speaking, the ridge finding algorithm moves points on the 2D grid according to the gradient of galaxy's distribution until these points arrive on ridges (please see Figure 2 of Chen et al. 2015b for an illustration). Note that we approximate the orientation of filaments using the density gradient so it may be slightly different from the actual orientation; the details of the approximation is in Chen et al. (2016). The average separation between points on a filament is about 0.77 Mpc. This can be viewed as the uncertainty due to the resolution of our filament finder. This uncertainty is much smaller than the uncertainty of filament's location due to sampling (around 10–20 Mpc; see Chen et al. 2016) so we can ignore its effect on the alignment signal. Note that increasing the grid density will improve the resolution of filament finder but will also increase the computational cost. We choose the grid density to be dense enough but still computationally feasible.

For each galaxy, we denote d_F as its distance to the nearest point representing filaments. This quantity will be a proxy for the distance to the closest filament. One can view d_F as the projected distance from a galaxy to the nearest filament in terms of angular diameter distance. More specifically, filaments in the Cosmic Web Reconstruction catalogue are constructed in each redshift slice. For a given galaxy, we first identify which redshift slice that it belongs to. Then we compute its distance to the nearest filament in the same

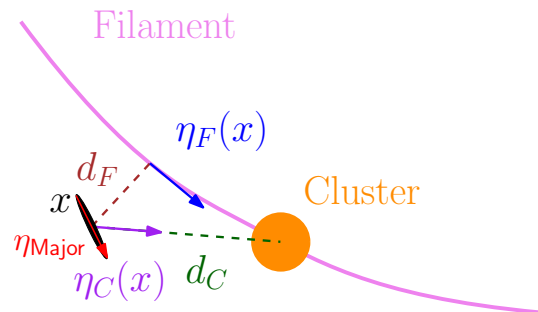


Figure 1. For a galaxy located at position x , this figure illustrates the quantities η_F (orientation of the nearby filament at the point nearest to the galaxy) and η_C (orientation of the unit vector connecting the galaxy and a cluster). The distance to the filament (d_F) is the length of the brown dashed line and the distance to the cluster (d_C) is the length of the green dashed line. Finally, η_{Major} shows the major axis direction of the projected galaxy shape.

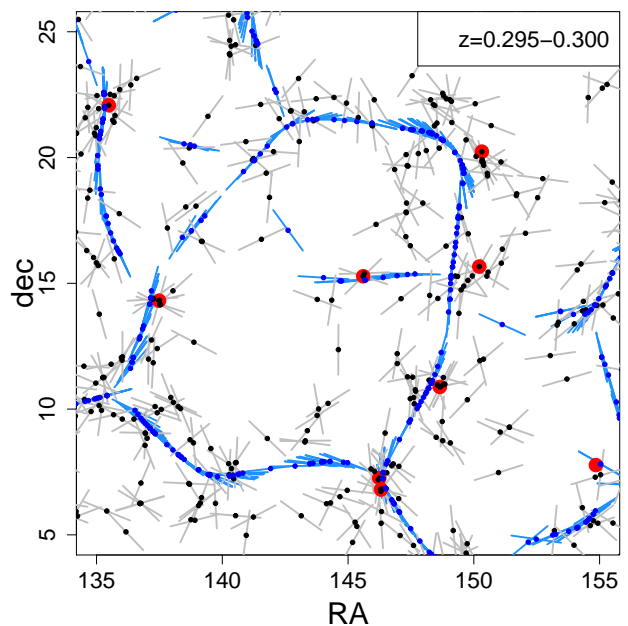


Figure 2. An illustration of galaxies (black dots), clusters (red dots), and filaments (curves, represented by dark blue dots) in a narrow redshift slice in the LOWZ sample. The gray lines on the galaxies indicate the direction of their major axes. The light-blue line segments indicate the orientation of the filament at the location of the dark blue dots. One degree on this figure corresponds to ~ 20 Mpc given the redshift indicated on the legend.

slice, disregarding the fact that galaxies near the borders between slices may be physically closer to filaments in an adjacent slice. This simplification may slightly reduce the significance of the observed alignment effects. Given a galaxy located at position x , we denote $\Pi_F(x)$ as its projected point onto the filament. Then the vector

$$\eta_F(x) = \eta_{\text{filament}}(\Pi_F(x)) \quad (3)$$

is defined as the orientation of the filament (unit vector tangential to the filament) nearest to the galaxy located at x . Similarly, for each galaxy, we define d_C and η_C as the distance and unit vector to the nearest redMaPPer cluster. [Figure 1](#) provides an illustration of the quantities η_F , η_C , d_F , and d_C for a given galaxy, filament, and cluster. For each galaxy, the primary shape-related quantity we are interested in is η_{Major} , the direction of the major principal axis of the galaxy projected onto the plane of the sky.

In [Figure 2](#) we show the distribution of galaxies, filaments and their shape orientations in a small region within the LOWZ sample ($0.295 < z < 0.300$). Our focus will be on understanding the alignments of the galaxies (gray lines) and the influence of filaments (blue lines) and clusters (red points) on these alignments. A notable feature in the figure is that the galaxies are primarily distributed close to the filaments and clusters, with clusters themselves being close to the filaments. This becomes important as we later split the galaxies into subsamples based on distances to filaments and clusters, where the samples with larger distance from clusters and filaments will have fewer galaxies, which increases the noise in the measurements.

3 RESULTS

3.1 Filament effect on galaxy-cluster alignment

Several studies have been performed to understand the galaxy alignments with surrounding density field using both observations and simulations (see e.g. [Kirk et al. 2015](#), for review) In this section, we investigate the effects of filaments on the galaxy-density alignment using clusters as the tracers of density field. We quantify the galaxy-cluster alignment with the statistic ([Zhang et al. 2009](#); [Tempel et al. 2013, 2015](#); [Chen et al. 2015c](#)):

$$|\phi_C - \phi_{\text{Major}}| = \arccos(|\eta_C \cdot \eta_{\text{Major}}|). \quad (4)$$

Namely, the quantity $\phi_C - \phi_{\text{Major}}$ is the angular difference between the the two axes η_C and η_{Major} . It can be computed by inverting the inner product $\eta_C \cdot \eta_{\text{Major}}$. Note that since we are comparing the angular difference of two axes, the value occurs between 0 degree (perfectly aligned) to 90 degrees (perfectly anti-aligned). For the case of random alignments, this quantity will be (uniformly) randomly distributed over the interval $[0, 90]$. We note that for the galaxies with low ellipticity the estimates of the direction of the major axis become noisier (for a round galaxy, the major axis direction is ill-defined). However, we do not apply any preferential treatment to low ellipticity galaxies in our analysis as this effect mainly adds to noise to our measurement.

We study the average alignment $\langle |\phi_C - \phi_{\text{Major}}| \rangle$ in two cases. (i): we fix d_F and study how $\langle |\phi_C - \phi_{\text{Major}}| \rangle$ changes as d_C changes; (ii): we fix d_C and study how $\langle |\phi_C - \phi_{\text{Major}}| \rangle$ changes as d_F changes. [Figure 3](#) shows the results for both cases; the error bars are based on the standard error of the average within each bin. In all cases, a statistically significant alignment of galaxies towards clusters is seen, but with different scale dependence. In the top row, we display the result of case (i). In the two leftmost panels ($0 \text{ Mpc} < d_F < 10 \text{ Mpc}$), we observe a significant dependence of the alignments on d_C , with the strength of the galaxy alignment toward the

cluster decreasing as the distance to the nearest cluster increases. This decreasing pattern is qualitatively consistent with the galaxy alignments literature where the alignments between galaxies and the density field follows a power law relation (see e.g. [Kirk et al. 2015](#), for a review of galaxy alignment measurements). The significance of the galaxy-cluster alignment measurements decreases as the distance to the filaments increases (two rightmost panels in top row of [Figure 3](#)). This trend is primarily driven by the increased noise as the number of galaxies decreases with the increased distance to filament and does not imply a significant filament effect on the galaxy-cluster alignment.

In the bottom row, we show the result of case (ii) to study the galaxy-cluster alignment as function of the distance of the galaxies to the filaments. We do not observe any significant dependence of galaxy alignments towards galaxy clusters on the distance to the filaments. These results suggest that filaments do not have a significant impact on the tendency of galaxies to align towards galaxy clusters.

3.2 Galaxy-filament alignment

In this section we investigate whether galaxies are aligned in parallel to nearby filaments. We define the filament orientation as the direction of the tangent at minimum separation from the galaxy (see [Figure 1](#)), which gives the alignment statistic

$$\langle |\phi_F - \phi_{\text{Major}}| \rangle = \arccos(|\phi_F - \phi_{\text{Major}}|). \quad (5)$$

Similar to the galaxy-cluster alignment measurement above, we now study how the galaxy-filament alignment changes as a function of distance to filaments d_F .

3.2.1 Separating impact of filaments and clusters

As shown in [Section 3.1](#), clusters influence the alignments of galaxies up to the maximum scale measured in this work, $d_C < 50 \text{ Mpc}$. [Figure 3](#) shows that the alignment effect of galaxies towards clusters is consistent with random at this distance and we therefore consider only galaxies with larger distances from the nearest cluster. [Figure 4](#) shows the alignment of galaxies in the parallel direction with respect to nearby filaments given a cluster-centric distance threshold of $> 50 \text{ Mpc}$. The parallel alignment signal is measured as a function of d_F , the distance to the nearby filament. In every panel, we see statistically significant detection at small values of d_F , with a decreasing alignment up to $30 - 40 \text{ Mpc}$ from the filament; linear regressions over the entire range in d_F yield significant detection of a negative slope in all three cases. The cut with $d_C > 50 \text{ Mpc}$ is particularly relevant because at this distance, the galaxy-cluster alignment becomes negligible (see [Figure 3](#)). Our interpretation of this finding is that filaments induce a coherent alignment signal that is not directly associated with clusters.

3.2.2 Range of galaxy-filament alignment effect

To determine the range of the filament alignment effect ρ_0 , we use the cutoff distance where the angular difference goes over 45 degrees (average of random alignment). Also note

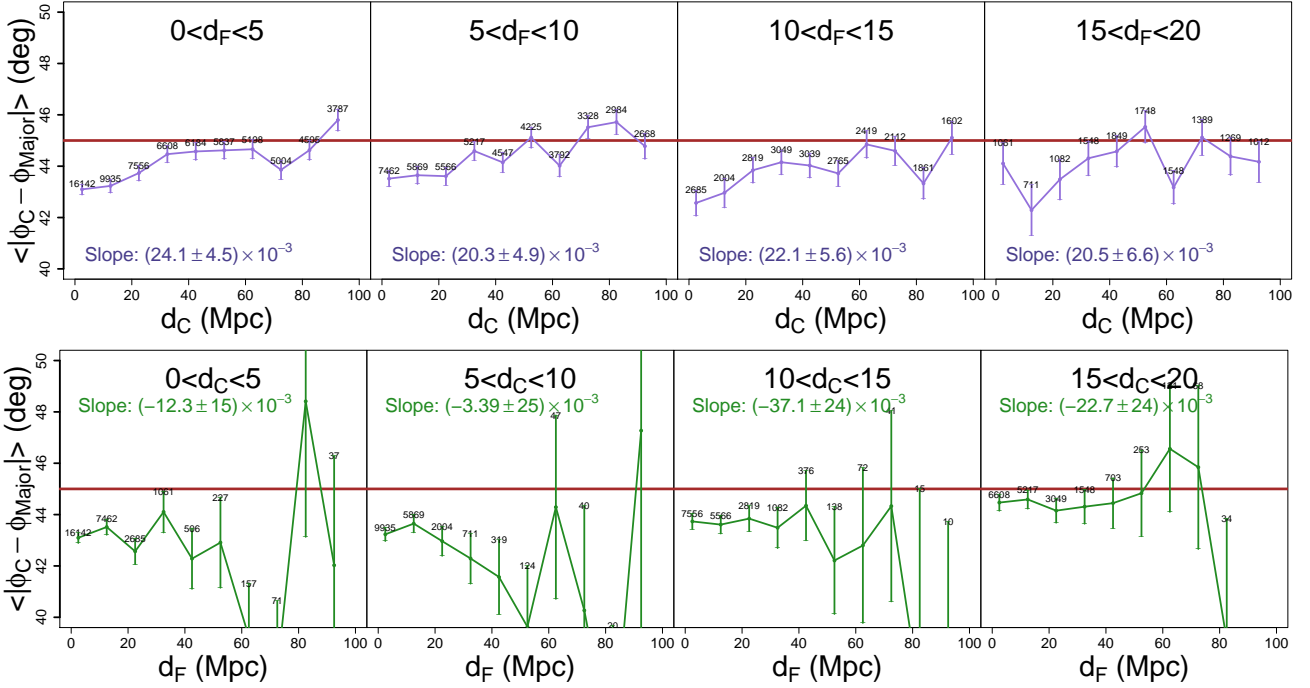


Figure 3. The galaxy alignment signal toward clusters $\langle |\phi_C - \phi_{\text{Major}}| \rangle = \langle \arccos|\eta_C \cdot \eta_{\text{Major}}| \rangle$ as a function of distance to the clusters, d_C and filaments, d_F . $\langle \cdot \rangle$ denotes the mean of the statistic. The numbers on the bins denotes the number of galaxies in each bin. The brown horizontal line indicates the average value from a random alignment. **Top panel:** the alignment towards clusters as a function of projected distance to the cluster at various (fixed) distances to filament as indicated on the plot. The slope is from fitting a linear regression to the scale- (distance-) dependence of the signal. In the first two panels, there is significant scale dependence of the alignment signal toward clusters. In the next two panels, measurements are noisier as the number of galaxies in bins decreases, making it harder to infer the scale dependence of the signal. But in all cases, we see that the curve is going up, indicating that clusters do have impact on the alignment of nearby galaxies. **Bottom panel:** the alignment toward clusters as a function of distance to filament at various (fixed) distances to the clusters. In this case we do not observe a significant scale dependence. Results from both panels suggest that the filaments do not have a significant impact on the alignment of galaxies toward clusters, within the uncertainty in the measurements. The fact that most parts of the curves are below 45 degrees (i.e., an alignment effect) is because we are only looking at galaxies that are very close to clusters (they are all below 20 Mpc to the cluster). These galaxies are greatly influenced by the effect of cluster.

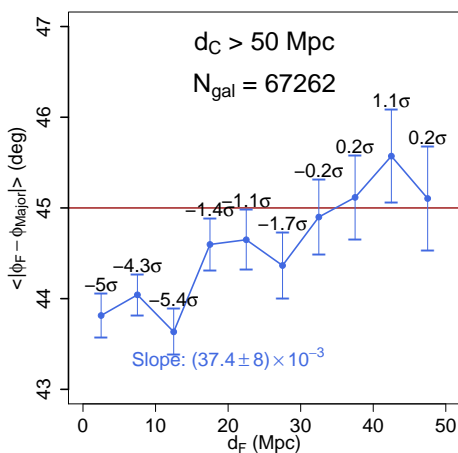


Figure 4. The galaxy-filament parallel alignment signal $\langle |\phi_F - \phi_{\text{Major}}| \rangle$ as a function of distance to the filament for galaxies with a cluster-centric distance d_C above 50 Mpc. We observe statistically significant galaxy-filament parallel alignment that decreases with separation from the filament, with a significant non-zero slope as indicated on the plot. The brown horizontal line indicates the average value from a random alignment.

that the value of ρ_0 could be due to uncertainty in filaments and does not necessarily imply some physical scale

We use the local polynomial regression (Wasserman 2006) as a non-parametric method to estimate the regression function. Given a value of covariate x (here the covariate is the distance to filament d_F), the local polynomial regression weights all the data points based on the distance from their covariate values to x . Close data points are given higher weights and far away data points are given less weights. In the local polynomial regression, there is a smoothing bandwidth b that determines how the weight as a distance to x decays. Roughly speaking, points within $[x - b, x + b]$ will have a much higher weight compared to those outside this window. One can view this approach as a modified method of fitting a regression based on taking the average over a sliding window of width $2b$. The reasons of using a local polynomial regression are that (i) it has a smaller statistical error compared to the conventional binning approach, and (ii) it does not require any prior knowledge about the shape of the regression function.

We present the results in Figure 5 with a bandwidth $b = 5$ Mpc; an analysis with different bandwidths yields comparable results. The top panel displays the fit results for 100 bootstrap samples; the bottom panel shows the distribution

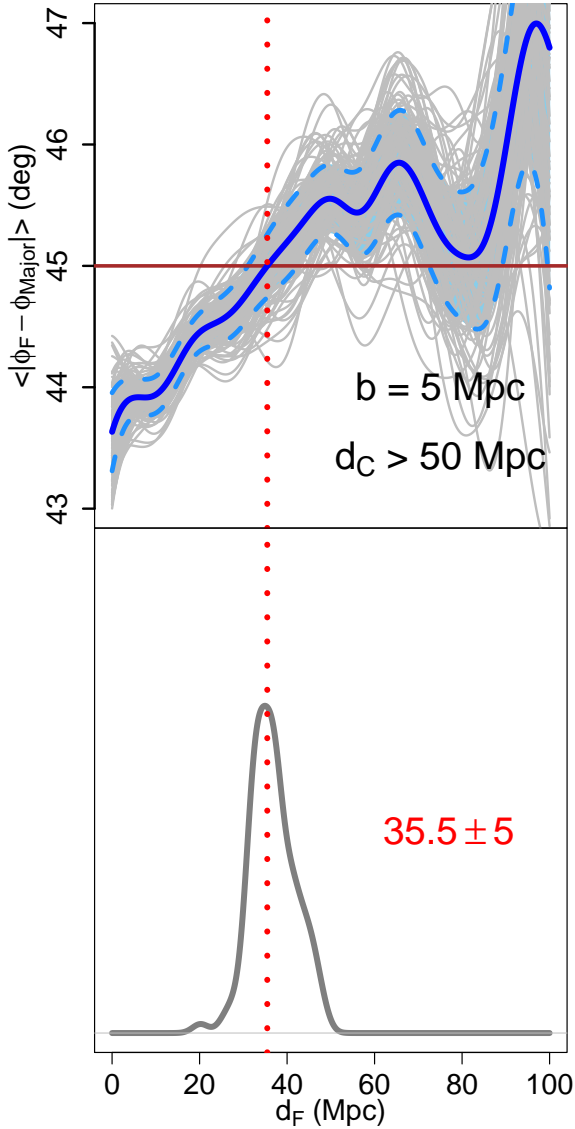


Figure 5. The range ρ_0 of the galaxy-filament parallel alignment effect for galaxies with a cluster-centric distance d_C above 50 Mpc. **Top:** The local polynomial regression fits with smoothing bandwidth $b = 5$ Mpc for 100 bootstrap samples (gray); their mean (blue); and their 90% pointwise confidence bands (cyan). **Bottom:** The probability density plot of ρ_0 from 100 bootstrap samples. The vertical dotted red line indicates the distance that the alignment signal first dropped to the average of random alignments.

of ρ_0 based on those bootstrap samples. In agreement with Figure 4, we find the range $\rho_0 \approx 35$ Mpc with a standard error of about 5 Mpc.

Using the range of the filament alignment effect, we calculate the excess probability density function of the difference angle $|\phi_F - \phi_{Major}|$, normalized to a pair of random axes. We only use galaxies within 40 Mpc, i.e. those that are within the range of the effect, with cluster-centric distances $d_C > 50$ Mpc. The results are shown in Figure 6, demonstrating that there are more galaxies aligned along their nearby filaments than one would expect from uniform random orientations.

Note that one may notice the anti-alignment at large

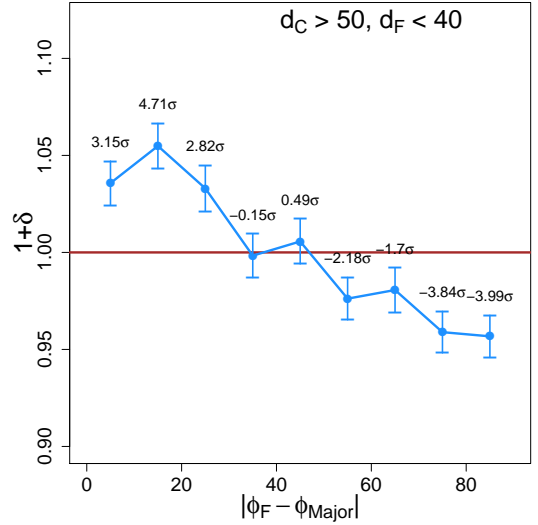


Figure 6. Excess probability density of the alignment in the parallel direction to nearby filaments for galaxies within the range of the filament alignment effect ρ_0 and cluster-centric distances d_C above 50 Mpc. $\delta = p_{obs}/p_{rand} - 1$, where p_{obs} is the probability density from observed alignments and p_{rand} is the probability density from random alignments.

	25%	15%	10%
Brightness	7.1×10^{-4}	4.8×10^{-3}	2.9×10^{-2}
Stellar Mass	7.5×10^{-2}	1.1×10^{-2}	5.0×10^{-2}
Age	3.0×10^{-2}	3.3×10^{-3}	6.8×10^{-2}

Table 1. P-value of testing the difference between the two extreme groups in Figure 7 using a χ^2 test. We highlight the case where the p-value is less than 0.05, a conventional threshold for claiming significance.

d_F (blue curve went over the brown horizontal line) in the top panel of Figure 5. Such an anti-alignment may be caused by the fact that when a galaxy is far away from a filament, the nearest filament can be viewed as a point source to this galaxy. We expect a galaxy to align toward a point mass, which explains why we observe the anti-alignment. To further examine such an effect, we analyze the alignment of those galaxies with $d_F > 50, 100$ Mpc in Section C. When we investigate those galaxies, we do not observe a significant alignment. So we cannot conclude if such an anti-alignment is a realistic effect from our study.

3.2.3 Galaxy properties and galaxy-filament alignment

To investigate whether the galaxy-filament alignment depends on galaxy properties, we perform the same analysis after separating galaxies by their absolute magnitude, stellar mass, and age. The stellar mass and age are obtained from the Granada group catalog (Ahn et al. 2014).³

When binning on each of these three properties in turn, we compare the two most extreme groups for a given

³ More details can be found at http://www.sdss.org/dr13/spectro/galaxy_granada/

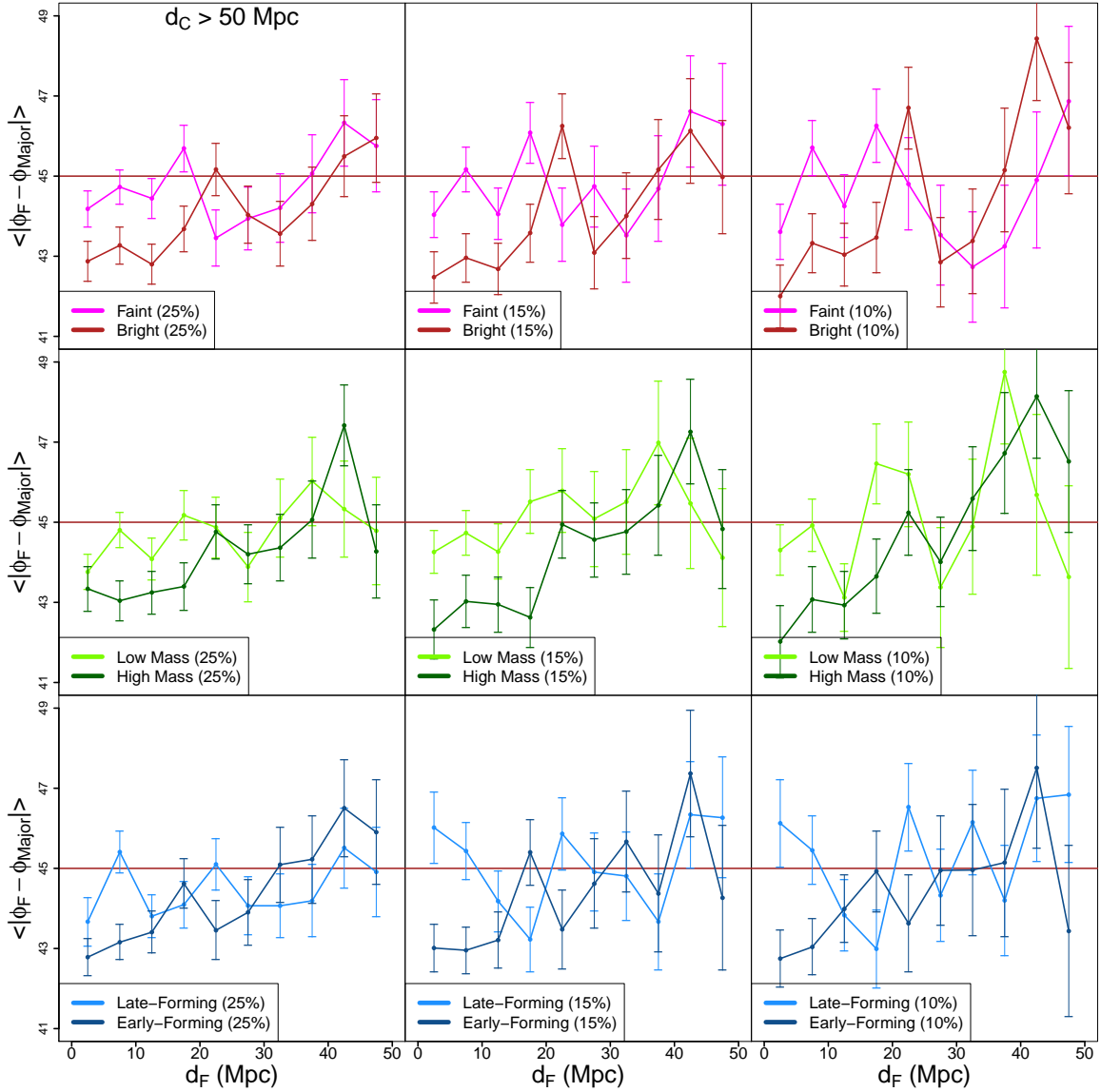


Figure 7. This figure shows the effect of galaxy properties on filament alignment. We compare the two most extreme groups of galaxies according to a particular galaxy property. From left to right, the extreme groups are selected with 25%, 15%, and 10% criteria. In all panels, we only consider galaxies with $d_C > 50$ Mpc to reduce the impact of cluster alignments. The p-value for the difference between the two extreme groups is given in Table 1. **Top row:** We separate galaxies by their brightness (r -band absolute magnitude). The upper and lower brightness thresholds are $(-22.16, -21.69)$, $(-22.31, -21.58)$, and $(-22.42, -21.50)$. **Middle row:** We separate galaxies by their stellar mass. The upper and lower mass thresholds are $\log_{10}(M_*/M_\odot) = (11.76, 11.55)$, $(11.83, 11.50)$, and $(11.87, 11.47)$. **Bottom row:** We separate galaxies by their age. The upper and lower age thresholds are $(8.38, 7.06)$, $(8.73, 6.59)$, and $(9.13, 6.41)$ Gyr.

property. For the brightness (r -band absolute magnitude), we compare the 25%/15%/10% brightest galaxies versus the 25%/15%/10% faintest galaxies, and likewise for stellar masses and ages. Note that the distribution of these properties in the LOWZ sample is relatively narrow, which means that even the extreme split performed here does not result in a very large difference between the samples.

To quantify the significance of the different alignment behavior between the two extreme groups of galaxies, we perform a simple χ^2 test by binning galaxies according to their distance to filaments (d_F). In what follows we describe the details of the χ^2 test we are using but essentially, it is the conventional χ^2 test with the bins described in Figure 7. Let

B_1, \dots, B_8 be the first 8 bins of d_F in Figure 7. Namely, B_ℓ contains galaxies with $5(\ell-1) \leq d_F < 5\ell$ Mpc, where ℓ is the bin index, ranging from 1–8. These bins corresponds to the galaxies with $d_F < 40$ Mpc. The upper bound 40 Mpc which is roughly the range of filament’s effect ρ_0 ; see Section 3.2.2. We use the following χ^2 statistic to test if the two extreme groups have consistent alignment behavior:

$$\chi^2 = \sum_{\ell=1}^8 \frac{(\langle |\phi_F - \phi_{\text{Major}}| \rangle_{\text{high}, \ell} - \langle |\phi_F - \phi_{\text{Major}}| \rangle_{\text{low}, \ell})^2}{\sigma_{\text{high}, \ell}^2 + \sigma_{\text{low}, \ell}^2}, \quad (6)$$

where $\langle |\phi_F - \phi_{\text{Major}}| \rangle_{\text{high}, \ell}$ is the average alignment of the highest group galaxies in bin ℓ and $\langle |\phi_F - \phi_{\text{Major}}| \rangle_{\text{low}, \ell}$ is that of the lowest group in bin ℓ . If there is no effect from the

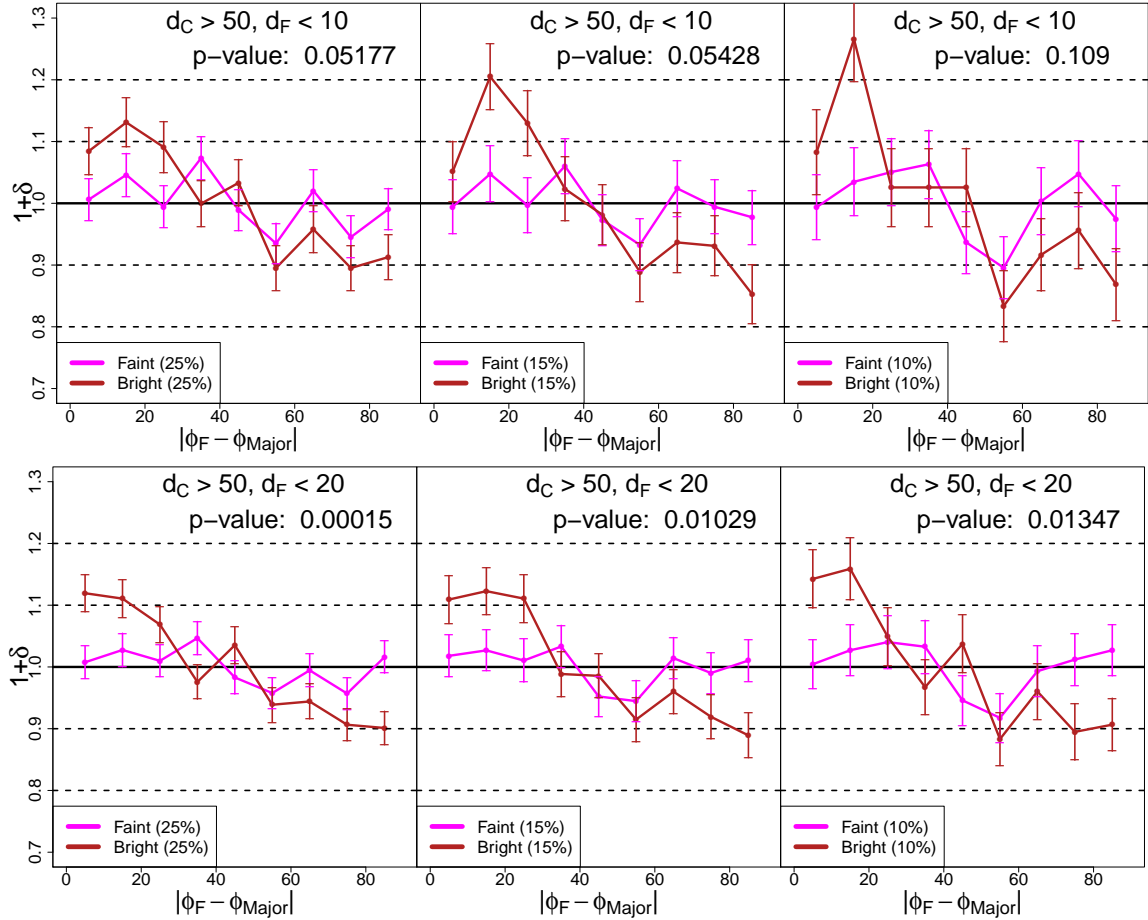


Figure 8. This figure shows the effect of brightness on the excess probability of galaxy-filament alignment. This figure is similar to the bottom row of Figure 6, but here we compare the brightest and dimmest galaxies while thresholding the maximum distance to filaments at 10 Mpc (top row) and 20 Mpc (bottom row). Note that the top right panel shows the p-value computed from a two-sample χ^2 test to examine whether the two groups (brightest versus faintest) have the same excess probability. We compare the brightest galaxies versus the faintest galaxies using the r -band magnitude. We observe a significance increase in the excess probability at smaller misalignment angles, indicating the presence of galaxy-filament alignment. Moreover, when we consider more extremely separated galaxy populations, the increase in excess probability at small misalignment angle seems to increase in amplitude (top row, from the left panel to the right panel).

specified galaxy property, we expect no statistically significant difference between the two extreme groups, and the χ^2 statistic will follow a χ_8^2 distribution (χ^2 distribution with degree of freedom 8). The results of this test for different galaxy properties and split criteria are displayed in Table 1.

In Figure 7, we show on the impact of galaxy properties on alignment with filaments. In the top row, we split galaxies on absolute magnitude and observe a separation between the two groups of galaxies, with bright galaxies more aligned along nearby filaments compared to faint galaxies. The χ^2 test shown in Table 1 confirms this pattern – the two samples have a difference with p-values ranging from 7.1×10^{-4} to 2.9×10^{-2} .

To further analyze how the brightness affects the alignment, we consider galaxies within 10 or 20 Mpc of a filament and at least 50 Mpc away from a cluster. We show the excess probability in terms of the angular difference $|\phi_F - \phi_{Major}|$ in Figure 8. For both filament distance thresholds shown in Figure 8, we observe a clear increase in excess probability at small angular difference, implying that the major axes of

both dim and bright galaxies tend to align along the orientation of nearby filaments. Moreover, the bright galaxies have a higher excess probability at the small angular difference, indicating that the galaxy-filament alignment is stronger for bright galaxies.

The age of a galaxy also has a significant impact on the alignment (bottom row of Figure 7). Early-forming galaxies that are close to a filament tend to align along the orientation of that filament whereas the alignment of late-forming galaxies seems to be independent of filaments. The χ^2 test in Table 1 shows a difference with p-values ranging from 3.3×10^{-3} to 6.8×10^{-2} . However, this effect may just be due to the effect of brightness and the correlation between age and brightness. Because we have a limited sample size, we do not adjust for the effect from brightness. When we separate galaxies by their age, the resulting galaxies have an age-brightness correlation ranging from 0.24 to 0.37. Thus, when partitioning on age of galaxies, the early-forming galaxies tend to be brighter than the late-forming galaxies and this brightness difference may cause the age effect.

The effect from stellar mass is more involved. The middle row of Figure 7 shows some small separations between the low mass and high mass galaxies in the sense that massive galaxies seem to have a stronger alignment effect. But the χ^2 analysis in Table 1 leads to a result that is close to the boundary of significance. The χ_8^2 statistics give p-values ranging from 1.1×10^{-2} to 7.5×10^{-2} , which is around the conventional significance level 0.05. Hence we detect some possible effects from the stellar mass, but the results are not as significant as those for brightness or age.

Note that in Section D, we apply the KS test and AD test (Anderson-Darling test) to compare the two most extreme groups. The results remain very similar to what was observed in Table 1.

4 CONCLUSION

In this work, we have studied how filamentary structure impacts the orientation of galaxies in the SDSS LOWZ sample. We quantified two different types of galaxy alignments: galaxy-cluster alignments and galaxy-filament alignments. Our primary results are as follows:

- **We find a statistically significant galaxy-filament alignment.** In the analysis of Section 3.2, we observed a significant tendency for galaxies to be oriented in a direction parallel to the nearest filament. Such an effect exists when we consider galaxies at least 50 Mpc away from clusters, to remove the impact of galaxy alignments towards clusters. Moreover, the analysis in Section 3.2.2 further indicates that the range of filament influence on the alignment is $\sim 30 - 45$ Mpc, though some of this effect appears to be determined by uncertainty in filament positions rather than a real alignment over tens of Mpc.
- **Galaxy brightness (absolute magnitude) and age impact the amount of alignment with filaments.** Our analysis in Section 3.2.3 shows that the brightness and age of a galaxy impact the effect of filaments on alignment, with brighter galaxies and/or those that are early-forming tending to be more aligned, especially when the distance to the filament is < 10 Mpc. Overall, our results are qualitatively consistent with previous work (Tempel et al. 2015 and Zhang et al. 2013) although the scale is very different.
- **We do not observe a significant impact of filaments on galaxy-cluster alignments.** In the analysis of Section 3.1, we find that the alignment of galaxies around clusters can be well explained by the distance to the cluster itself, and there is no statistically significant contribution from filaments. However, we note that such an effect may exist at a level too weak to be detected in our data.
- **We find weak evidence for the galaxy-filament alignment strength to depend on stellar mass.** When we separate galaxies according to their stellar mass, we only observe a difference in the galaxy-filament alignment that is on the boundary of significance. We do not observe a very significant effect as the findings of Zhang et al. (2009) and Chen et al. (2015c). However, as before, differences in galaxy samples and methodology may account for this difference. Our results indicate that galaxy alignments are impacted by the complexity of large-scale structure beyond the positions of the most massive objects (clusters). We leave for future

work an assessment of whether existing models for galaxy alignment, which typically treat correlations with the total density field or within the halo environment, are sufficient to account for the impact of filaments. Models that explicitly treat density-filament correlations may improve the overall description of galaxy alignments. Potential inconsistencies with previous results highlight the value of performing similar analyses on future data sets with greater statistical power.

ACKNOWLEDGMENTS

We are grateful for the useful comments made by the referee. YC is supported by NIH grant number U01 AG016976. SH is supported by NASA ROSES grant 12-EUCLID12-0004 and NASA ROSES grant 15-WFIRST15-0008 and [nsf-ast 1517593](#). JB acknowledges the support of an Ambizione Fellowship from the Swiss National Science Foundation. RM is supported by NSF grant number AST-1716131.

Funding for SDSS-III has been provided by the Alfred P. Sloan Foundation, the Participating Institutions, the National Science Foundation, and the U.S. Department of Energy Office of Science. The SDSS-III web site is <http://www.sdss3.org/>.

SDSS-III is managed by the Astrophysical Research Consortium for the Participating Institutions of the SDSS-III Collaboration including the University of Arizona, the Brazilian Participation Group, Brookhaven National Laboratory, Carnegie Mellon University, University of Florida, the French Participation Group, the German Participation Group, Harvard University, the Instituto de Astrofísica de Canarias, the Michigan State/Notre Dame/JINA Participation Group, Johns Hopkins University, Lawrence Berkeley National Laboratory, Max Planck Institute for Astrophysics, Max Planck Institute for Extraterrestrial Physics, New Mexico State University, New York University, Ohio State University, Pennsylvania State University, University of Portsmouth, Princeton University, the Spanish Participation Group, University of Tokyo, University of Utah, Vanderbilt University, University of Virginia, University of Washington, and Yale University.

REFERENCES

- Abazajian K. N., et al., 2009, *ApJS*, **182**, 543
 Ahn C. P., et al., 2012, *ApJS*, **203**, 21
 Ahn C. P., et al., 2014, *ApJS*, **211**, 17
 Aihara H., et al., 2011, *ApJS*, **193**, 29
 Alam S., et al., 2015, *ApJS*, **219**, 12
 Altay G., Colberg J. M., Croft R. A. C., 2006, *MNRAS*, **370**, 1422
 Aragon-Calvo M. A., Yang L. F., 2014, *MNRAS*, **440**, L46
 Aragón-Calvo M. A., van de Weygaert R., Jones B. J. T., van der Hulst J. M., 2007, *ApJ*, **655**, L5
 Aragón-Calvo M. A., van de Weygaert R., Jones B. J. T., 2010, *MNRAS*, **408**, 2163
 Blanton M. R., Lin H., Lupton R. H., Maley F. M., Young N., Zehavi I., Loveday J., 2003, *AJ*, **125**, 2276
 Blazek J., MacCrann N., Troxel M. A., Fang X., 2017, preprint (arXiv:1708.09247),
 Bolton A. S., et al., 2012, *AJ*, **144**, 144
 Cautun M., van de Weygaert R., Jones B. J. T., 2013, *MNRAS*, **429**, 1286

- Chen Y.-C., Genovese C. R., Wasserman L., 2015a, *The Annals of Statistics*, **43**, 1896
- Chen Y.-C., Ho S., Freeman P. E., Genovese C. R., Wasserman L., 2015b, *MNRAS*, **454**, 1140
- Chen Y.-C., et al., 2015c, *MNRAS*, **454**, 3341
- Chen Y.-C., Ho S., Brinkmann J., Freeman P. E., Genovese C. R., Schneider D. P., Wasserman L., 2016, *MNRAS*, **461**, 3896
- Conroy C., Gunn J. E., White M., 2009, *ApJ*, **699**, 486
- DES Collaboration et al., 2017, preprint (arXiv:1708.01530),
- Dawson K. S., et al., 2013, *AJ*, **145**, 10
- Forero-Romero J. E., Hoffman Y., Gottlöber S., Klypin A., Yepes G., 2009, *MNRAS*, **396**, 1815
- Fukugita M., Ichikawa T., Gunn J. E., Doi M., Shimasaku K., Schneider D. P., 1996, *AJ*, **111**, 1748
- Ganeshiah Veena P., Cautun M., van de Weygaert R., Tempel E., Jones B. J. T., Rieder S., Frenk C. S., 2018, preprint, p. arXiv:1805.00033 (arXiv:1805.00033)
- Gunn J. E., et al., 1998, *AJ*, **116**, 3040
- Gunn J. E., et al., 2006, *AJ*, **131**, 2332
- Hahn O., Porciani C., Carollo C. M., Dekel A., 2007a, *MNRAS*, **375**, 489
- Hahn O., Carollo C. M., Porciani C., Dekel A., 2007b, *MNRAS*, **381**, 41
- Hahn O., Carollo C. M., Porciani C., Dekel A., 2007c, *MNRAS*, **381**, 41
- Hildebrandt H., et al., 2017, *MNRAS*, **465**, 1454
- Hirata C., Seljak U., 2003, *MNRAS*, **343**, 459
- Hogg D. W., Finkbeiner D. P., Schlegel D. J., Gunn J. E., 2001, *AJ*, **122**, 2129
- Ivezic Ž., et al., 2004, *Astronomische Nachrichten*, **325**, 583
- Joachim B., et al., 2015, *Space Sci. Rev.*, **193**, 1
- Kilbinger M., 2015, *Reports on Progress in Physics*, **78**, 086901
- Kirk D., et al., 2015, *Space Sci. Rev.*, **193**, 139
- Komatsu E., et al., 2011, *ApJS*, **192**, 18
- Libeskind N. I., Hoffman Y., Forero-Romero J., Gottlöber S., Knebe A., Steinmetz M., Klypin A., 2013, *MNRAS*, **428**, 2489
- Mandelbaum R., 2017, preprint, (arXiv:1710.03235)
- Ozertem U., Erdogmus D., 2011, *Journal of Machine Learning Research*, **12**, 1249
- Padmanabhan N., et al., 2008, *ApJ*, **674**, 1217
- Reid B., et al., 2016, *MNRAS*, **455**, 1553
- Reyes R., Mandelbaum R., Gunn J. E., Nakajima R., Seljak U., Hirata C. M., 2012, *MNRAS*, **425**, 2610
- Rozo E., Rykoff E. S., 2014, *ApJ*, **783**, 80
- Rozo E., Rykoff E. S., Bartlett J. G., Melin J.-B., 2015, *MNRAS*, **450**, 592
- Rykoff E. S., et al., 2014, *ApJ*, **785**, 104
- Schneider M. D., Bridle S., 2010, *MNRAS*, **402**, 2127
- Singh S., Mandelbaum R., More S., 2015, *MNRAS*, **450**, 2195
- Smee S. A., et al., 2013, *AJ*, **146**, 32
- Smith J. A., et al., 2002, *AJ*, **123**, 2121
- Sousbie T., Pichon C., Colombi S., Novikov D., Pogosyan D., 2008, *MNRAS*, **383**, 1655
- Tempel E., Libeskind N. I., 2013, *ApJ*, **775**, L42
- Tempel E., Stoica R. S., Saar E., 2013, *MNRAS*, **428**, 1827
- Tempel E., Guo Q., Kipper R., Libeskind N. I., 2015, *MNRAS*, **450**, 2727
- Wasserman L., 2006, *All of Nonparametric Statistics*. Springer-Verlag New York, Inc.
- York D. G., et al., 2000, *AJ*, **120**, 1579
- Zhang Y., Yang X., Faltenbacher A., Springel V., Lin W., Wang H., 2009, *ApJ*, **706**, 747
- Zhang Y., Yang X., Wang H., Wang L., Mo H. J., van den Bosch F. C., 2013, *ApJ*, **779**, 160
- Zhang Y., Yang X., Wang H., Wang L., Luo W., Mo H. J., van den Bosch F. C., 2015, *ApJ*, **798**, 17

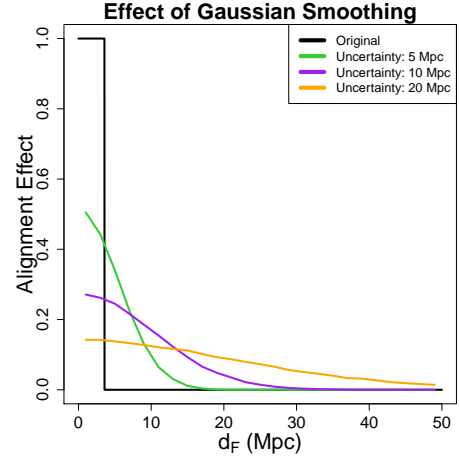


Figure A1. A simple model to analyze the effect of filament uncertainty on the observed galaxy-filament alignment effect. The black curve describes a simple model for the alignment effect: within a distance 3.5 Mpc, the effect has a magnitude 1 and 0 otherwise. We then smooth this effect by a different amount of Gaussian uncertainty (5, 10, and 20 Mpc) and display how the alignment effect may be extended to a longer distance. The uncertainty of filaments in the Cosmic Web Reconstruction is around 10 – 20 Mpc in the LOWZ sample (Chen et al. 2016). Based on this simple model, the alignment effect may last to 30 – 50 Mpc, which is consistent with what we observed in Figure 4.

APPENDIX A: EFFECT FROM FILAMENT UNCERTAINTY

To investigate the effect from filament uncertainty, we consider a very simple model where the alignment effect is

$$\begin{cases} 1, & \text{if } d_F \leq 3.5 \text{ Mpc,} \\ 0, & \text{if } d_F > 3.5 \text{ Mpc.} \end{cases}$$

The threshold 3.5 Mpc is from the study in simulations in Chen et al. (2015c). To model the impact of uncertainty in the filament position, we assume that our observed distance to filament

$$d_{F,\text{obs}} = |d_F + \epsilon|,$$

where d_F is the true distance to filament and ϵ is a random number follows from a Normal distribution with variance σ^2 . We consider $\sigma = 5, 10$, and 20 Mpc and we display the result on the alignment signal in Figure A1. The uncertainty of filaments in the LOWZ sample is about 10–20 Mpc according to Chen et al. (2016), model predictions with $\sigma = 10$ and 20 Mpc provide a rough idea for how the Gaussian uncertainty distance to the filament affects the range of effect. According to Figure A1 the uncertainty of filaments may lead to an alignment effect with a range up to 50 Mpc, which is close to what we observed in Figure 4. Moreover, the magnitude reflects how the alignment effect was damped by the uncertainty. When the uncertainty is around 10 – 20 Mpc, the alignment effect is reduced to 1/4 – 1/6 of the original alignment effect.

APPENDIX B: CHECKING FOR THE SYSTEMATICS

In this section, we investigate possible systematics using two approaches. The first one is to study the systematics from the distribution of filaments' orientations (ϕ_F). The other one is to study the alignment of galaxies when they are far away from both filaments and galaxies.

Ideally, the distribution of filaments' orientations should be close to a uniform distribution. However, as is shown in the top-left panel of Figure B1, the distribution has bumps at ± 90 deg ($\phi_F = \pm 90$ deg, the direction along RA direction), indicating that we have more filaments along the RA direction than the dec direction. This is probably due to the artifact of the survey geometry, where the ranges of RA is much wider than the range of dec, making the boundary along RA direction larger than along the dec direction. Thus, our filament finders will tend to detect more filaments along the long boundary (RA direction) than the short boundary (dec direction). To further examine the boundary bias, we consider galaxies and filaments within the region $150^\circ < RA < 200^\circ$ and $10^\circ < dec < 30^\circ$. This region is chosen because it is in the interior of the LOWZ sample area. We compute the orientations of filaments in the top-right panel. The two bumps around ± 90 deg get damped and the distribution is more randomly fluctuating, which suggest that the boundary bias may be the main driving force for the two bumps. Note that the fluctuation in this panel may be due to the cosmic variance since we are using a small region in the sky.

Although there are artifacts in filaments' orientations, the distribution of ϕ_{Major} is very uniformly distributed (bottom-left panel of Figure B1). To investigate if the artifacts of filaments' orientation will cause systematics in galaxy-filament alignments, we randomly shuffle the redshift slices of filaments and compute the alignment signal. Namely, galaxies in redshift slice A may be compared to filaments from redshift slice B. If there is no systematics, we will not observe any alignment signal. In the bottom-right panel of Figure B1, we see that the result is consistently with random orientations, which suggests that there is no strong evidence of systematics from different redshift slices.

To examine if there are systematics within the same redshift slice, we randomly pair a galaxy to a filament within the same slice, regardless of their distance. For each pair of galaxy-filament, we compute the angular difference between the galaxy's major axis and the filament's orientation. The result is given in the left panel of Figure B2. Clearly, the result is consistent with a flat line, suggesting that there is no evidence about the systematics within the same redshift slice. As a reference, we attach the result when we pair a galaxy to the nearest filament in the right panel (this is our alignment signal). We observed a significant increase of probability in the aligned cases (low value of $|\phi_F - \phi_{\text{Major}}|$), which suggests the presence of galaxy-filament alignments.

Finally, to examine possible systematics caused by coordinate transformations, we separate the data into two parts according to the declination: one sample with a high declination ($> 24^\circ$) and the other one with a low declination ($< 24^\circ$). Note that the threshold 24 degrees is chosen based on the median declination of the entire LOWZ sample. For each sample, we apply the same technique to detect the alignment

signal and the result is given in Figure B3. In both cases, we observe a significant alignment when the distance to filament is small and the alignment disappears when the distance to filament is large, which is consistent with the observations in Figure 4. And the trends in both panels are very consistent. The fact that there is no clear difference between the low declination and high declination samples suggest that no systematics from coordinate transformations.

APPENDIX C: CHECKING FOR THE ANTI-ALIGNMENT

In Figure 5, we notice that there seems to be an anti-alignment effect when d_F is large (however, it is not statistically significant). To investigate if such an anti-alignment is realistic, we analyze the alignments of galaxies toward filaments for those galaxies that are far away from both filaments and clusters.

In particular, we consider galaxies with $d_C > 50$ Mpc and $d_F > 50, 100$ Mpc and investigate the distribution of $\phi_{\text{Major}} - \phi_F$. The result is given in Figure C1. The distribution is very similar to a uniform distribution in both cases and the KS test gives p-values 0.07 (when we threshold $d_F > 50$ Mpc) and 0.86 (when we threshold $d_F > 100$ Mpc). Thus, we do not observe a significant effect in our sample so we cannot conclude if there is indeed an anti-alignment effect when galaxies are far away from filaments.

APPENDIX D: P-VALUES FROM OTHER TESTS

In addition to the χ^2 test, we also employ the KS test and AD test to investigate if galaxy's properties have a significant impact on the alignment signal. We focus on the comparison in Section 3.2.3 and Figure 7 and re-create Table 1 with the other two tests. The p-values are given in Table D1. Note that for the ease of comparison, we also include the results from Table 1 (χ^2 test).

In every test, there are six scenarios where a significant difference is observed: separating galaxies by the most extreme 25% or 15% brightness, the most extreme 15% stellar mass, and the most extreme 25%, 15%, or 10% age. In particular, when galaxies are separated by their brightness or age, we see very significant differences in some cases (for instance, the 25% extreme brightness or the 15% extreme age comparison) across every test.

This paper has been typeset from a $\text{\TeX}/\text{\LaTeX}$ file prepared by the author.

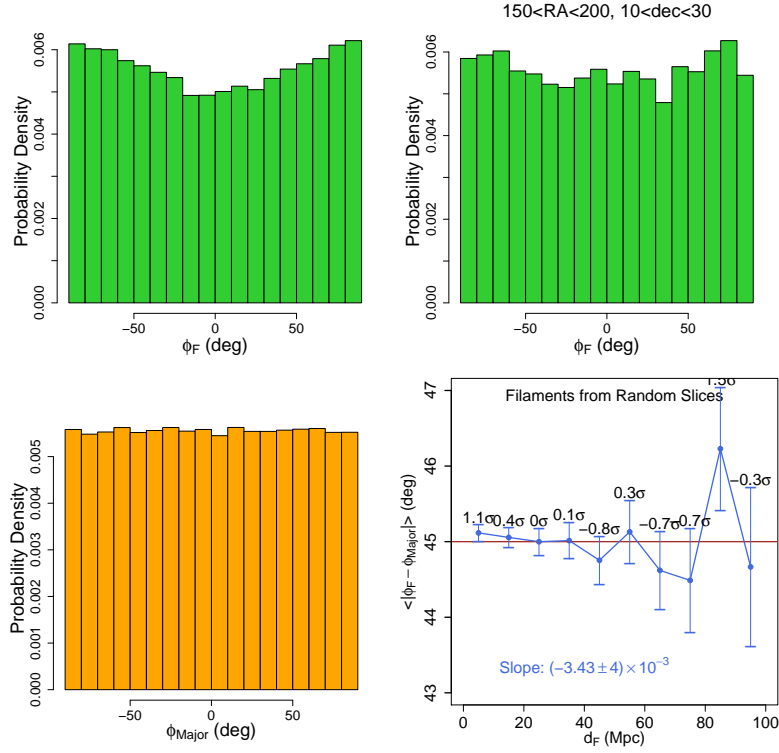


Figure B1. We examine the distributions of filaments' orientations (ϕ_F) and the major axes of galaxies (ϕ_{Major}). In the top-left panel, we see that the orientation of filaments are not very uniformly distributed but instead, there are more filaments with an orientation parallel to the RA direction (close to ± 90 degrees). This may be caused by the boundary bias of the filament finder – ridgelines are constructed by applying the kernel density estimator, which is known to have a higher statistical bias around the boundary of the data. In the top-right panel, we attempt to study examine the boundary bias by focusing the region inside $150 < RA < 200$, $10 < dec < 30$ and computing the filaments' orientation. This regions is completely inside the survey area of the LOWZ sample so the boundary bias will be limited. Although there are some fluctuations in this panel, there is no clear pattern as in the top-left panel. The fluctuation may be caused by cosmic variance. In the bottom-left panel, we display the distribution of major axes of galaxies, which follows a uniform distribution. In the bottom-right panel, we randomly shuffle the redshift slices of filaments and calculate the alignment signal. We observe a flat line, indicating that there is no systematics in our analysis.

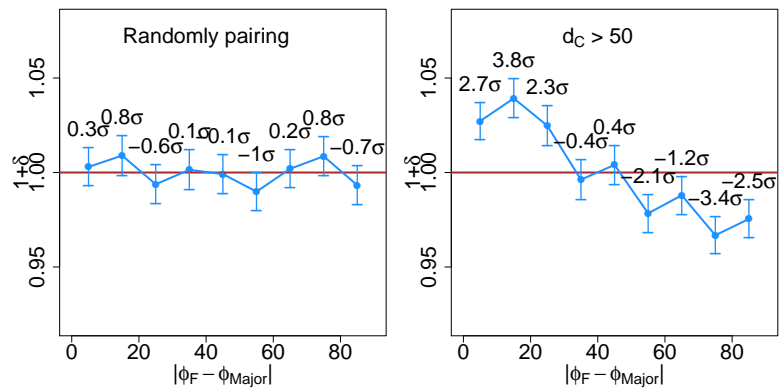


Figure B2. Examining the within-slice systematics using excess probability distribution ($\delta = 1 - \frac{P_{\text{obs}}}{P_{\text{rand}}}$). **Right panel:** To examine the systematics, we randomly pair a galaxy to a filament within the same redshift slice and compute the angular difference between the major axis of the galaxy and the orientation of the filament. Here, the excess probability distribution is consistent with a flat line, suggesting that there is no strong evidence of systematics. **Left panel:** This is a reference to the right panel. This panel shows the results when we pair a galaxy to the nearest filament (with a constraint that galaxies have to be at least 50 Mpc away from clusters to eliminate the effect from clusters). We observe an increase in probability in aligned cases (low value of $|\phi_F - \phi_{\text{Major}}|$), suggesting the presence of galaxy-filament alignments.

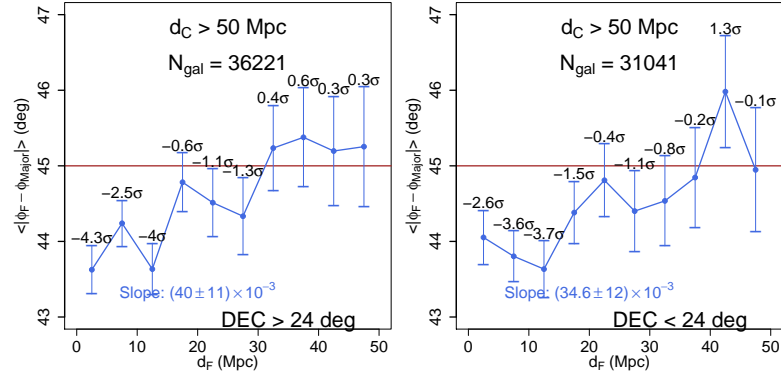


Figure B3. Examining the systematics from coordinate transformations by splitting the data according to the declination. We separate the galaxy sample by the declination into two samples: a high declination sample and a low declination sample. We then compute the alignment signal as Figure 4. We observe a consistent pattern in both panels and the trend is very quantitatively similar to the one described in Figure 4.

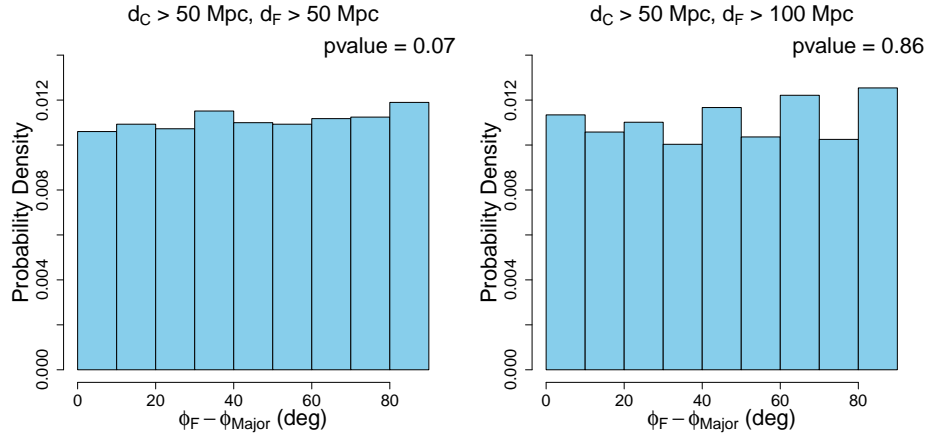


Figure C1. We check the systematics by considering galaxies that are far away from both clusters and filaments. In the top panel, we consider galaxies with $d_C > 50$ Mpc and $d_F > 50$ Mpc and in the bottom panel, we investigate those with $d_C > 50$ Mpc and $d_F > 100$ Mpc. We apply the KS-test to check if the distribution is significantly different from 0. The p-values are 0.07 and 0.86, both are not significant to the standard significance level 0.05.

(KS test)	25%	15%	10%
Brightness	3.6×10^{-3}	2.6×10^{-2}	1.3×10^{-1}
Stellar Mass	1.1×10^{-1}	2.2×10^{-2}	7.7×10^{-2}
Age	4.4×10^{-2}	2.8×10^{-3}	1.7×10^{-3}
(AD test)	25%	15%	10%
Brightness	4.0×10^{-4}	6.3×10^{-3}	7.1×10^{-2}
Stellar Mass	4.1×10^{-2}	4.1×10^{-3}	5.6×10^{-2}
Age	2.5×10^{-3}	4.3×10^{-3}	4.7×10^{-3}
(χ^2 test)	25%	15%	10%
Brightness	7.1×10^{-4}	4.8×10^{-3}	2.9×10^{-2}
Stellar Mass	7.5×10^{-2}	1.1×10^{-2}	5.0×10^{-2}
Age	3.0×10^{-2}	3.3×10^{-3}	6.8×10^{-2}

Table D1. Test for the significance between the two most extreme types of galaxies by different properties with different testing approaches. In the top table, we use the KS-test. In the middle table, we use the AD test. In the bottom table, we use the χ^2 test, which is the same as Table 1.